J Stat Phys (2013) 153:270–288
DOI 10.1007/s10955-013-0827-4

Complex Network Structure of Flocks in the Standard Vicsek Model

Gabriel Baglietto · Ezequiel V. Albano · Julián Candia

Received: 17 February 2013 / Accepted: 8 August 2013 / Published online: 5 September 2013

Abstract In flocking models, the collective motion of self-driven individuals leads to the formation of complex spatiotemporal patterns. The Standard Vicsek Model (SVM) considers individuals that tend to adopt the direction of movement of their neighbors under the influence of noise. By performing an extensive complex network characterization of the structure of SVM flocks, we show that flocks are highly clustered, assortative, and non-hierarchical networks with short-tailed degree distributions. Moreover, we also find that the SVM dynamics leads to the formation of complex structures with an effective dimension higher than that of the space where the actual displacements take place. Furthermore, we show that these structures are capable of sustaining mean-field-like orientationally ordered states when the displacements are suppressed, thus suggesting a linkage between the onset of order and the enhanced dimensionality of SVM flocks.

Keywords Self-propelled particle systems · Collective motion · Complex networks · Vicsek model

G. Baglietto · E.V. Albano · J. Candia (✉)
Instituto de Física de Líquidos y Sistemas Biológicos, CONICET, UNLP, 59 Nro 789, 1900 La Plata, Argentina
e-mail: juliancandia@gmail.com

G. Baglietto
Facultad de Ingeniería, UNLP, La Plata, Argentina

G. Baglietto
Physics Laboratory, Istituto Superiore di Sanità, Gr. Coll. Roma I, V.le Regina Elena 299, 00161 Roma, Italy

E.V. Albano
Departamento de Física, Facultad de Ciencias Exactas, UNLP, La Plata, Argentina

J. Candia
Department of Physics, University of Maryland, College Park, MD 20742, USA

1 Introduction

Nature presents us with an astonishing variety of swarming and flocking phenomena spanning a huge range of lengthscales and organismal complexity, from bacterial colonies and migrating cells to insects swarms [1–5], from fish schools and shoals to bird flocks and mammal herds [6–10], extending even to crowd dynamics in human collective behavior [11, 12]. Therefore, it is hardly surprising the enormous interest that swarming phenomena has attracted across scientific disciplines, involving not just biologists, but also mathematicians, physicists, and engineers. Indeed, the modeling of swarming and flocking behavior contributes to the understanding of natural phenomena and becomes relevant for many practical and technological applications as well, e.g. collective robotic motion, design and control of artificial microswimmers, microscopic chemical robots (also known as *chobots*), etc. [13–17] (see Ref. [18] for a recent review).

In this broad context, the model early proposed by Vicsek et al. [19], i.e. the so-called Standard Vicsek Model (SVM), has gained large popularity within the Statistical Physics community, which uses it as an archetypical model to study the onset of order upon the interactive displacement of self-driven individuals. The SVM assumes that individuals tend to align their direction of movement when they are placed within a certain interaction range. This rule, which would trivially lead to a fully ordered collective motion, is complemented by a second one that introduces noise in the communications (interactions) among individuals. The interplay and competition between these simple rules leads to the observation of a rather complex and interesting nonequilibrium behavior: an ordered phase of collective motion is found for low enough levels of noise, while a disordered phase is observed at high noise levels. Further interest in the SVM arises from the fact that the nature of the phase transition between those phases could be physically described as first- or second-order, depending on the type of noise considered [19–23].

The SVM, which describes a far-from-equilibrium phenomenon, has been compared with the XY model, a widely studied critical system that operates under equilibrium conditions [24]. The XY model considers nearest-neighbor interacting spins that may adopt any possible orientation depending on the interplay between temperature and the nearest-neighbor interaction strength [25, 26]. By interpreting the SVM as a model of interacting "spins" that can undergo displacements in the direction of the spin, the basic difference between both models lies precisely in the SVM's spin displacements. In fact, other relevant symmetries for the study of phase transitions, such as the dimensionality of the space, the nature of the order parameter, and the range of the interactions, are the same in both models. On the other hand, it is well known that, according to the Mermin-Wagner Theorem [27–29], the XY model, as well as other equilibrium systems sharing the same symmetries, cannot exhibit large-scale ordered states in 2 dimensions. Therefore, the onset of ordering in the SVM in $2D$ is quite intriguing and has become the subject of several studies. Using a variety of approaches such as hydrodynamic equations [30], long-range links in ad-hoc complex network substrates [21], and off-lattice simulations [31], it has been shown that particle displacements in the SVM play the role of effective long-range interactions.

Within this context, the aim of this paper is to investigate the structural characteristics of the complex networks formed by clusters of self-driven individuals during the far-from-equilibrium stationary states of the SVM. By means of standard topological measures borrowed from the growing field of complex network research, we perform an extensive characterization of the structure of SVM flocks and link our findings to intrinsic characteristics of the SVM dynamics. Furthermore, we also investigate how the complex networks formed as a consequence of the particle displacements can still support the onset of orientational ordering once those displacements are suppressed (i.e. after *freezing* the clusters). Since, after

suppressing the displacements of the individuals, the SVM is essentially analogous to the XY model defined on complex network substrates, we interpret the onset of local ordering in terms of topological features of the frozen clusters that form the "spin" system's substrates.

This manuscript is organized as follows: in Sect. 2, we define the model, describe the computer simulation method and how the complex networks are obtained; Sect. 3 is devoted to the presentation and discussion of the results; while our conclusions are stated in Sect. 4. Finally, the Appendix presents the analytic calculation of the clustering coefficient for SVM flocks in the large-cluster asymptotic limit.

2 The Standard Vicsek Model

The Standard Vicsek Model (SVM) is perhaps the simplest model that captures the essence of collective motion in a non-trivial way [19]. It consists of a fixed number of interacting particles, N, which are moving on a plane. The particles move off-lattice with constant and common speed $v_0 \equiv |\vec{v}|$. Each particle interacts locally and tends to adopt the direction of motion of the subsystem of neighboring particles (within an interaction circle of radius R_0 centered in the considered particle). Since the interaction radius is the same for all particles, we define it as the unit of length throughout, i.e. $R_0 \equiv 1$.

The updated direction of motion for the ith particle, θ_i^{t+1}, is given by

$$\theta_i^{t+1} = \mathrm{Arg}\left[\sum_{\langle i,j\rangle} e^{i\theta_j^t}\right] + \eta\xi_i^t, \tag{1}$$

where η is the noise amplitude, the summation is carried over all particles within the interaction circle centered at the ith particle, and ξ_i^t is a realization of a δ-correlated white noise uniformly distributed in the range between $-\pi$ and π. The noise term can be thought of as due to the error committed by the particle when trying to adjust its direction of motion to the averaged direction of motion of their neighbors. Although several variations to the SVM have later been considered in the literature, such as different noise types, models without alignment rule, adhesion between neighbor individuals, bipolar particles, etc. (see [18] for a review), in this work we focus on the original SVM as formulated by Vicsek et al. in their seminal article [19].

We implement the model dynamics by adopting the so-called *backward update rule*: after the position and orientation of all particles are determined at time t, we update the position of the particles at time $t+1$ according to

$$\vec{x}_i{}^{t+1} = \vec{x}_i{}^t + \vec{v}_i{}^t, \tag{2}$$

which is then followed by the update of all velocities at time $t+1$ according to Eq. (1). For a detailed discussion on the impact of different updating rules, see Ref. [22].

The SVM exhibits a far-from-equilibrium phase transition between ordered states of motion at low noise levels and disordered motion at high noise levels. This order-disorder transition is manifested by the natural order parameter of the system, namely the absolute value of the normalized mean velocity of the system, given by

$$\varphi = \frac{1}{N v_0}\left|\sum_{i=1}^{N} \vec{v}_i\right|, \tag{3}$$

where φ is close to zero in the disordered phase and grows up to one in the ordered phase. Although the topic remains somewhat controversial, evidence suggests that the phase transition associated with the onset of large-scale ordered flocks is second-order, at least for the type of noise and update rule used in this work. For recent discussions on the subject, see e.g. Refs. [22, 32, 33].

The Standard Vicsek Model is studied by means of simulations implemented as a cellular automaton, where all particles update their states simultaneously in one time step. The particles move off-lattice in a $2D$ square of side $L = \sqrt{N/\rho}$, where ρ is the particle density. We adopted $N = 32768$, $v_0 = 0.1$, and $\rho = 0.25$ throughout. For these parameter values (which are standard in the Vicsek model literature), the critical point takes place at the noise amplitude $\eta_c = 0.134$ [34], although we explored a range of other noise values as well. It should be also pointed out that scaling relations near the transition region have been reported, which therefore link the behavior of different model parameters. For instance, noise amplitude and density at criticality are known to scale as $\eta \sim \sqrt{\rho}$ [34]. Since we were interested in stationary configurations, we started out our simulations with random initial states and disregarded the first 2×10^6 time steps. As pointed out in Ref. [31], the order parameter remains unchanged by taking any smaller value for the velocity amplitude v_0 (which only affects the duration of the transient period, i.e. the time needed to achieve stationary configurations).

After reaching the stationary regime, we determined the set of connected clusters by means of the Hoshen-Kopelman algorithm [35] adapted for the case of off-lattice systems. In order to build a set of complex networks that represent the stationary flocks generated by the SVM dynamics, we defined that two individuals were linked if the distance between them was within the interaction radius R_0. Hence, complex networks representing flocks in the stationary regime are non-weighted and undirected.

We have also investigated the onset of orientation ordering in so-called *frozen clusters* (see Sect. 3.4). Clusters of individuals were first generated using the full SVM dynamics, as explained above. However, once the stationary flocks were obtained, particle displacements (Eq. (2)) were suppressed. In these frozen clusters, individuals were still allowed to change their orientation following Eq. (1), with a noise amplitude in the range $0 < \eta_f < 1$, but their locations in space remained fixed.

3 Results and Discussion

Earlier studies on the Vicsek Model have shown that, starting with a disordered initial state in which individuals are randomly distributed, the dynamic rules lead to the formation of local structures of interacting individuals [19, 20]. These structures, which we will call *flocks* or *clusters* throughout, are not permanent: their shape and size evolve with time, with new individuals and sub-flocks merging with them and, conversely, other individuals and sub-flocks separating from them. Indeed, the process of merging and dismemberment of sub-flocks can be regarded as an effective long-range interaction, since via this mechanism the information of one part of the system may be carried to a different region of space [21, 30]. Although individual clusters do change with time, the statistical properties of the ensemble of clusters are constant once we disregard the initial transient regime. Hence, at any given time, statistical measurements taken over the flock ensemble are representative of the Vicsek Model's stationary state. Besides this statistical perspective, in which flocks are the fundamental building blocks of the flock ensembles that characterize SVM stationary states, flocks can be regarded as "domains" that carry important information on the ordering of the system at the mesoscopic level. Bearing in mind these two different perspectives on the role of flocks

or clusters as key sub-units within a SVM system, we will alternate between the structural analysis of single clusters and the analysis of flocks from the statistical ensemble approach.

In order to perform an extensive topological characterization of the flocks formed in the stationary phase of the Vicsek Model, we will use the complex network approach, which provides us with a conceptual framework and a set of measures that have been applied to a huge variety of networked systems from such diverse scientific realms as biology, ecology, sociology, physics, computer science, engineering and technology, finance and economics, and others [36–38]. By means of this approach, we identify connected clusters or flocks as the basic units of the system and measure their structural properties following well-established procedures from the complex network literature. As will be shown below, these measurements allow us to characterize the topology of SVM flocks, relate them to other networked systems, and understand their ability to sustain ordered states.

3.1 Cluster Structure and Size Distribution

Figure 1 shows the complex network structure of typical flocks in the stationary regime of the Standard Vicsek Model. In this complex network representation, the length of the links does not correspond to the actual physical distance between neighbor particles. Notice, however, that the intrinsic modularization of the network structure carries significant spatial information. For instance, one can observe two distinct modules that correspond to actual sub-flocks merging into (or separating from) each other. Indeed, flock collision and dismemberment have been identified as mechanisms that play a major role in the SVM dynamics [22].

Nodes are colored according to their degree: nodes with fewer connections than average ($k/\langle k\rangle < 1$) are shown in white, those slightly more connected than average ($1 \leq k/\langle k\rangle < 2$)

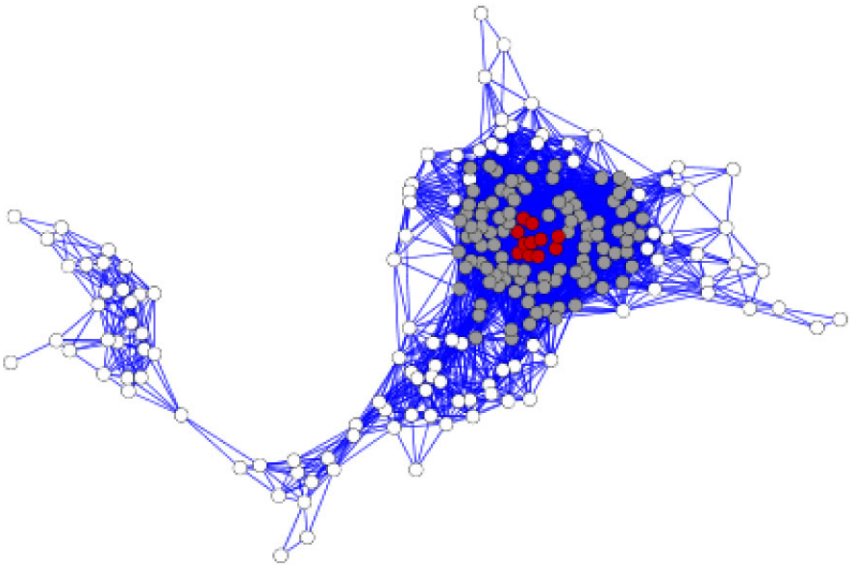

Fig. 1 Complex network structure of a typical SVM flock with 226 nodes, 4147 links, and mean degree $\langle k\rangle = 36.7$. The length of the links does not represent the actual physical distance between neighbor particles. Node colors indicate their degree: *white* ($k/\langle k\rangle < 1$), *grey* ($1 \leq k/\langle k\rangle < 2$), and *red* ($2 \leq k/\langle k\rangle < 3$). This complex network visualization was created with Cytoscape [39] (Color figure online)

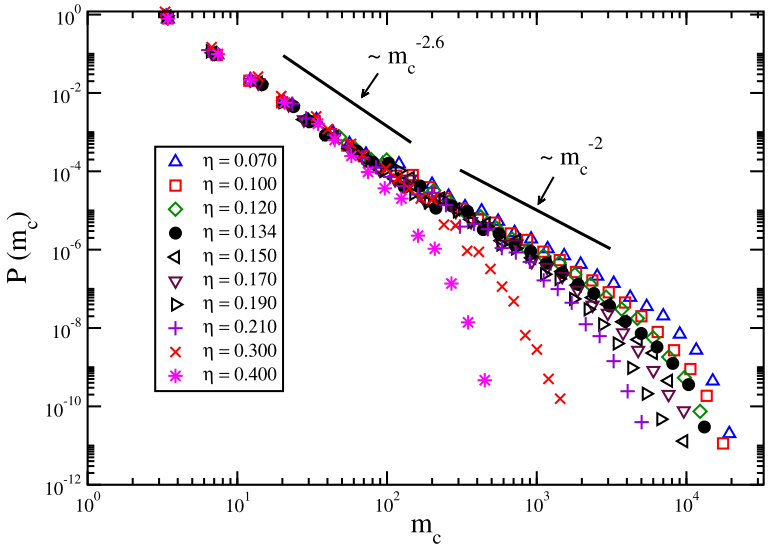

Fig. 2 Cluster mass probability distributions for different levels of noise, as indicated. The critical noise is $\eta_c = 0.134$ (Color figure online)

in grey, and the highly connected ones ($2 \leq k/\langle k \rangle$) in red. In the flock of Fig. 1, 95 % of the nodes fall in the first two categories, and there are no hubs with $k/\langle k \rangle \geq 3$. We observe a central core formed by the highly connected nodes, which is wrapped within layers of nodes that are less and less connected towards the flock periphery. There are no distinguishable nodes that monopolize most of the links (i.e. network hubs), meaning that there are no leaders guiding the flock as a whole. Moreover, we observe that leaves (i.e. nodes with just one neighbor) are very uncommon: only one leaf exists in the graph of Fig. 1, which appears on the far left. Notice also the abundance of triangles, which indicates high local clustering.

In SVM stationary configurations, connected clusters (such as the network shown in Fig. 1) are observed over a very wide range of sizes. The probability distribution of cluster masses is shown in Fig. 2 for different noise values, as indicated. Notice that, here and throughout this paper, we define the mass of a connected cluster, m_c, as the number of its constituent nodes. Over a wide range of noise values both below and above the critical point $\eta_c = 0.134$, the distributions follow power-laws that cross over to exponential decay tails. As expected, the power-law span is larger for smaller noise values. The exponents that characterize the power-law distributions $P(m_c) \sim m_c^{-\beta_c}$ lie in the range $2 \leq \beta_c \leq 2.6$. For much smaller systems, Huepe and Aldana [40] had found $\beta_c \simeq 1.5$ (for $N = 500$) and $\beta_c \simeq 1.9$ (for $N = 5000$), so we conclude that the mass cluster distribution exponents exhibit rather strong finite-size effects.

In order to gain insight into the structure of the clusters, let us first evaluate the average path length, *APL* [41, 42]. According to the standard definition used in the study of complex networks, for each pair of nodes (A, B) belonging to the same cluster, the path length ℓ_{AB} (also known as chemical distance) is given by the minimum number of links that one has to use in order to pass from one node to the other. Notice that, in networks with undirected links, this distance is the same in both directions. By calculating all the pairwise node-to-node path lengths in the cluster and taking the average, one obtains the *APL*, which consequently is a characteristic length of the cluster.

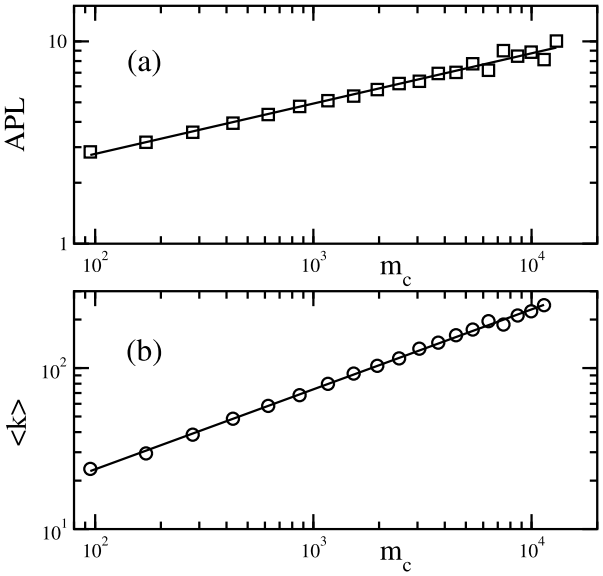

Fig. 3 (**a**) Log-log plot of the average path length *APL* as a function of the cluster size m_c with $\eta_c = 0.134$. The fit of Eq. (4) to the data yields $D = 4.0(2)$. (**b**) Log-log plot of the average degree $\langle k \rangle$ as a function of the cluster size m_c at the critical noise value $\eta_c = 0.134$. By fitting Eq. (5) to the data, we obtain $\alpha = 0.50(1)$

In Euclidean lattices, the volume of an object is related to its characteristic length by an integer power, i.e. the dimension of the object. Based on this observation, as well as on the experience gained in the study of fractal objects, it is customary to define the dimension (D) of a complex network according to:

$$APL \propto m_c^{1/D}, \tag{4}$$

where m_c is the complex network size or, in the present context, the cluster mass [42]. Figure 3(a) shows a log-log plot of the *APL* versus m_c for SVM flocks with $\eta_c = 0.134$, i.e. clusters corresponding to the critical point of the second-order phase transition. The best fit to the data yields $D = 4.0(2)$, which strongly suggests that the effective dimension of the clusters is $D = 4$.

Another quantity of interest for the characterization of complex networks is the average degree distribution as a function of the cluster mass [41, 42]. Figure 3(b) shows a log-log plot of $\langle k \rangle$ versus m_c, which demonstrates a power-law behavior, i.e.

$$\langle k \rangle \propto m_c^{\alpha}, \tag{5}$$

where $\alpha = 0.50(1)$.

The average degree is only the first moment of a more general property of a network, namely the degree distribution $P(k)$, defined as the probability of a vertex to have k links. We evaluated $P(k)$ vs k for different cluster mass ranges, as shown in Fig. 4 for flocks generated at the critical noise value $\eta_c = 0.134$. Notice that, by scaling the horizontal axis by the average degree, all curves collapse, thus indicating that clusters of all sizes have a self-similar structure. Analogous results (not shown here for the sake of space) are obtained by analyzing clusters in the network ensemble corresponding to the ordered phase (i.e. $\eta < \eta_c$).

The collapsed distribution is short-tailed with most nodes having degrees less than $3\langle k \rangle$. Indeed, as noticed above when discussing the structure of individual clusters (Fig. 1), flocks are not guided by leaders, thus the short-tailed nature of the degree distribution as opposed

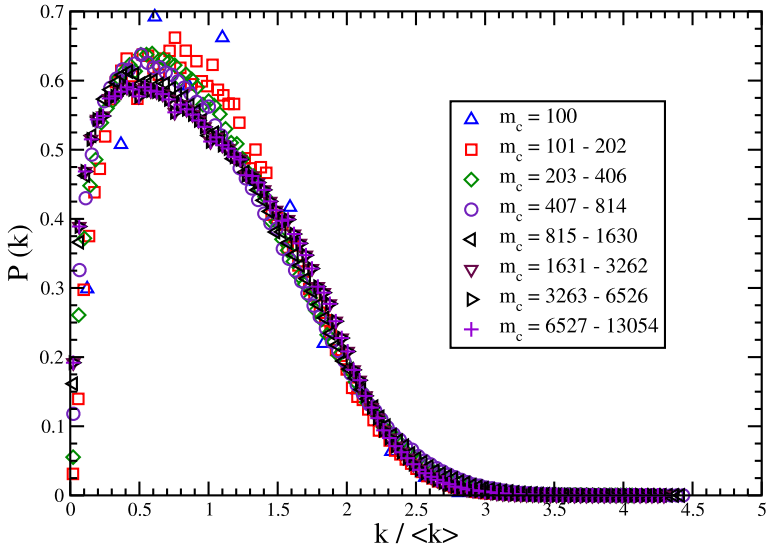

Fig. 4 Degree probability as a function of the normalized degree, obtained at the critical noise value $\eta_c = 0.134$ and for different cluster mass ranges, as indicated (Color figure online)

to scale-free-like structures characterized by the existence of hubs. Notice, however, that despite the short-tailed feature, the observed distribution does not match a Poisson distribution. In fact, Poisson degree distributions are characteristic signatures of classical random graphs, which also show small local clustering and a substantial fraction of leaves, while SVM flocks display high local clustering and a negligible fraction of leaves. We conclude that the short-tailed SVM distribution is a result of geographical constraints due to the interaction radius cutoff, which prevents the emergence of scale-free topologies.

3.2 Effective Dimension of Flocking Clusters

In the previous section, we found through Eq. (4) that SVM clusters have an effective dimension $D = 4$. Moreover, the average degree was found to scale with the cluster mass as $\langle k \rangle \propto m_c^{1/2}$, Eq. (5). Based on these observations, we will now conjecture that these results can be rationalized in terms of a projection of a $D = 4$ dimensional object into a $d = 2$ dimensional space.

Let us explore the effective topology of SVM clusters by considering the compactification of a hypercubic regular lattice of dimension D and m_c nodes. Hence, we begin with a hypercube of side $L = m_c^{1/D}$ and coordination number k_D, as shown in Fig. 5. If we compactify it once, keeping the same number of nodes but projecting them into a hypercube of side L and $D - 1$ dimensions, the coordination number is increased to $k_{D-1} \approx k_D \times L$. Notice that we can think of this process by assuming that each particle (node) in the original hypercube is slightly displaced at random off its corresponding lattice site, so that, after the projection, we obtain increased local densities without any two particles sharing exactly the same position. Indeed, the compactification process generates "particle lumps" that are responsible for the enhanced effective coordination number. After projecting multiple times (from the original D dimensions into a d-dimensional hypersurface), the coordination num-

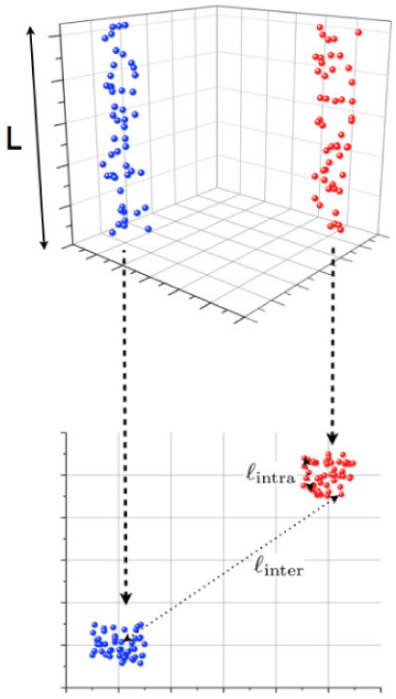

Fig. 5 Schematic representation of the compactification process, which leads to lower-dimensional structures with enhanced effective coordination numbers that scale according to Eq. (7) and average path length given by Eq. (4). Two clusters of nodes are shown in *blue* and *red*, as well as the characteristic lengthscales L, ℓ_{inter}, and ℓ_{intra}. See more details in the text (Color figure online)

ber becomes

$$k_d \approx k_D L^{D-d}, \tag{6}$$

or, by replacing the relation $L = m_c^{1/D}$,

$$k_d \propto m_c^{\frac{D-d}{D}}. \tag{7}$$

On the other hand, we can estimate the average path length of the compactified d-dimensional object. This object has side L and lumps formed by $n_d = m_c/L^d$ nodes around each one of the L^d lattice sites. As shown in Fig. 5, the distance between nodes that belong to the same lump is of the order of unity: $\ell_{\text{intra}} \sim \mathcal{O}(1)$. However, node pairs that belong to different lumps have $\ell_{\text{inter}} \sim \mathcal{O}(L)$ on average. Thus,

$$\ell \sim \begin{cases} \mathcal{O}(1) & \text{for } n_d(n_d-1)/2 \times L^d \text{ node pairs,} \\ \mathcal{O}(L) & \text{for } n_d^2 \times L^d(L^d-1)/2 \text{ node pairs.} \end{cases} \tag{8}$$

Hence, the leading contribution to the average path length is due to node pairs in different lumps and $APL \equiv \langle \ell \rangle \propto L$, which agrees with Eq. (4) after replacing $L = m_c^{1/D}$. In this way, by taking $D = 4$ and $d = 2$, the compactification mechanism leads to node clusters that have $APL \propto m_c^{1/4}$ (from Eq. (4)) and $\langle k \rangle \propto m_c^{1/2}$ (from Eq. (7)), in agreement with the exponents measured for SVM clusters. Let us point out that the behavior of L as a function of m_c signals the presence of a nontrivial scaling law for the areas of the clusters. In fact, $L \propto m_c^{1/4}$ is compatible with areas that grow as $m_c^{1/2}$ instead of lineary in m_c.

Summing up, in this section we focused our attention on the average degree and characteristic length of clusters of different mass. Our heuristic arguments show that SVM clusters

can be understood as 4-dimensional networked objects compactified into a 2-dimensional space. As will be discussed below (see Sect. 3.4), these arguments are also useful in order to understand the onset of long-range ordering in frozen clusters.

3.3 Clustering Coefficient Analysis of SVM Flocks

A very important topological measure of a complex network is the clustering coefficient, C [41, 42]. The clustering coefficient for node i with k_i links is defined as

$$C_i = \frac{2n_i}{k_i(k_i - 1)}, \tag{9}$$

where n_i is the number of links between the k_i neighbors of i. Then, the network's clustering coefficient is calculated as the average of C_i taken over all vertices, i.e. $C = \langle C_i \rangle$. Empirical results over a wide variety of real networks have shown that C is significantly higher for most real networks than for corresponding random networks of similar size [41, 43, 44]. Furthermore, the clustering coefficient of real networks is to a high degree independent of the number of nodes in the network. Interestingly, however, the archetypical complex network models predict a marked drop of the clustering coefficient with the network size N. For instance, classical random graphs have $C = \langle k \rangle / N$, while the Barabási-Albert scale-free model leads to $C \sim N^{-0.75}$ [41].

Figure 6 shows the dependence of C on m_c. Notice that flocks of all sizes display a very high degree of clustering, as we anticipated based on the high density of triangles observed in the network structure from Fig. 1. Also, we observe that the size dependence is very weak: fitting the scaling relation $C \propto m_c^{-\gamma}$, we obtain $\gamma = 0.025(1)$.

As shown in the Appendix, the asymptotic clustering coefficient in the limit of an infinitely large cluster, C_∞, can be calculated as a function of the density of particles inside the cluster, ρ_{in}, according to

$$C_\infty = \frac{[(4\pi - 3\sqrt{3})\rho_{\text{in}} - 8]\pi\rho_{\text{in}}}{4(\pi\rho_{\text{in}} - 1)(\pi\rho_{\text{in}} - 2)}, \tag{10}$$

which is expected to be an excellent approximation in the case of large clusters where the surface-to-bulk ratio is negligible. Since the scaling relation $\langle k \rangle \sim m_c^{0.5}$ implies that

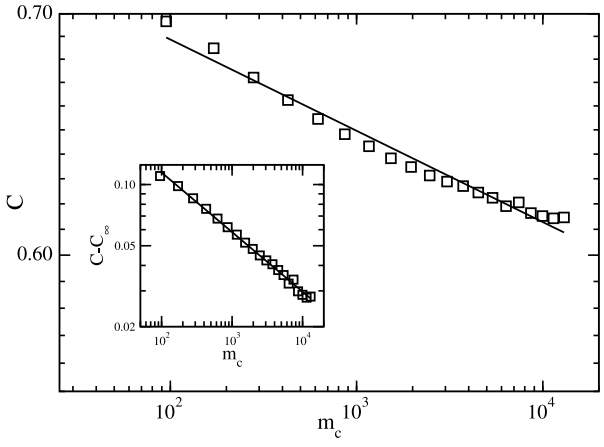

Fig. 6 Log-log plot of the clustering coefficient C as a function of the cluster size m_c. *Inset*: after subtracting the asymptotic clustering coefficient C_∞, the exponent $\gamma_\infty = 0.30(2)$ is determined

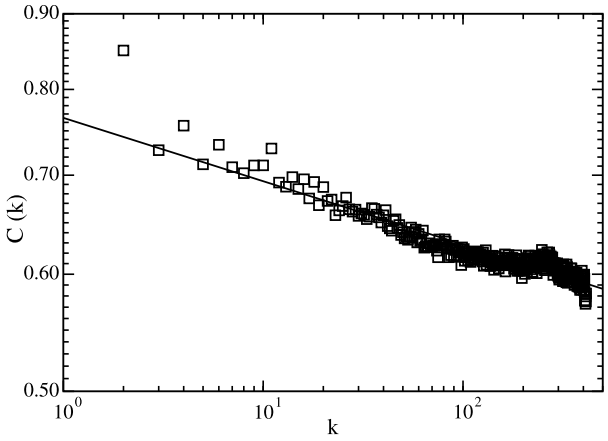

Fig. 7 Log-log plot of the clustering coefficient $C(k)$ as a function of the degree k. Due to their strong geographical constraints, flocks have a nonhierarchical network topology

$\rho_{\text{in}} \to \infty$ in the $m_c \to \infty$ limit, Eq. (10) yields

$$C_\infty = 1 - \frac{3\sqrt{3}}{4\pi} \simeq 0.587. \tag{11}$$

The inset to Fig. 6 shows a log-log plot of $C - C_\infty$ as a function of the cluster mass m_c, where it is shown that $C - C_\infty$ decays with m_c as a power law with exponent $\gamma_\infty = 0.30(2)$.

In order to determine whether modular organization is responsible for the high clustering coefficients seen in many real networks, Ravasz et al. [45, 46] introduced the scaling law

$$C(k) \propto k^{-\beta_h}, \tag{12}$$

where $C(k)$ represents the distribution of the clustering coefficient as a function of the node degree and β_h is the exponent that measures the hierarchical structure of complex networks. Indeed, it has been observed that many real networks are composed of modules that combine into each other in a hierarchical manner. These hierarchical networks are uncovered by a scaling behavior of $C(k)$ that follows Eq. (12) with $\beta_h \simeq 1$. Figure 7 shows a log-log plot of $C(k)$ as a function of the degree. The drop with the degree is very mild, namely $\beta_h = 0.043(1)$, which is also compatible with a logarithmic decay. This result points to a lack of hierarchical organization in the network structure of flocks. We argue that, since links in the network construction process are distance-driven and limited by spatial constraints (namely, that particles must lie within an interaction radius R_0 in order to be connected), the emergence of a hierarchical topology is prevented.

Another important network characterization is the degree of assortative mixing, i.e. whether high-degree vertices are preferentially attached to other high-degree vertices (in which case the network is termed assortative) or whether, on the contrary, high-degree vertices are preferentially attached to low-degree ones (in the case of disassortative networks) [47, 48]. Most often, social networks are assortatively mixed, while technological and biological networks tend to be disassortative. Network models such as classical random graphs and Barabási-Albert scale-free networks are neither assortative nor disassortative.

One way to determine the degree of assortative mixing is by considering the average degree $\langle k_{\text{NN}} \rangle$ calculated among the nearest-neighbors of a node of degree k. Figure 8 show a log-log plot of the $\langle k_{\text{NN}} \rangle$ vs k distribution, which reveals a very high degree of assortative mixing. Indeed, by fitting the data to a power-law of the form $\langle k_{\text{NN}} \rangle \propto k^{\gamma_a}$, the assortativity

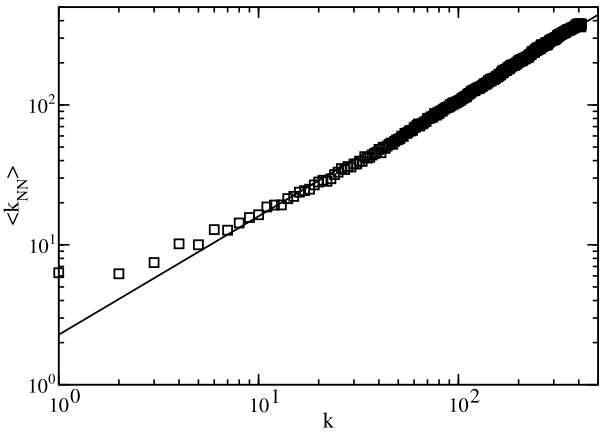

Fig. 8 Log-log distribution of the average degree $\langle k_{\rm NN}\rangle$ of nearest-neighbors of nodes of degree k, which reveals that SVM flocks have a highly assortative network topology

exponent turns out to be $\gamma_a = 0.848(4)$. Alternatively, one can measure the degree of assortativity as the Pearson correlation coefficient of the degrees at either ends of an edge. This measure, originally introduced by Newman [47], is obtained from the expression

$$r = \frac{1}{\sigma_q^2}\sum_{ij} ij\,(e_{ij} - q_i q_j), \tag{13}$$

where i, j are the degrees of the vertices at the ends of a given edge and the summation is carried over all edges in the network. Instead of using a node's degree k_i, here we are interested in the node's *remaining degree* $q_i = k_i - 1$ that excludes the edge between the two nodes being considered. Moreover, e_{ij} is the joint probability distribution of the remaining degrees of the two vertices at either end of a randomly chosen edge [49], and $\sigma_q^2 = \sum_k k^2 q_k - [\sum_k k q_k]^2$ is the variance of the q_k distribution. The definition of r through Eq. (13) lies in the range $-1 \le r \le 1$, with assortative networks having $r > 0$ and disassortative ones having $r < 0$. For instance, several scientific collaboration networks show assortative mixing in the range $0.12 \le r \le 0.36$, while the network of connections between autonomous systems on the Internet has $r = -0.19$ and the food web from undirected trophic relations in Little Rock Lake, Wisconsin has $r = -0.28$ [47]. The Pearson correlation coefficient measured among large flocks turns out to be $r_A = 0.82(6)$, i.e. SVM flocks have very high assortative mixing.

As mentioned above, it is well known that high local clustering and high assortativity are distinct hallmarks of social networks. Moreover, the imitation mechanism between neighboring interacting particles introduced by the SVM dynamics resembles well-studied "ferromagnetic"-like interactions that play a key role in the occurrence of social cooperative phenomena [50, 51]. Hence, these observed structural properties of SVM flocks can be interpreted as arising from the social nature that underlies the behavior of individuals according to the SVM dynamics.

3.4 Onset of Orientation Ordering in Frozen Clusters

One of the most intriguing features of the SVM is the onset of long-range ordering and the existence of an order-disorder phase transition in $d = 2$ dimensions. In order to explore this phenomenon, here we analyze whether the topology of frozen clusters, once particle displacements and cluster rearrangements are suppressed, is capable by itself of supporting the

existence of an orientationally ordered phase. For this purpose, we first generate configurations of clusters by applying the full SVM dynamics. Once the non-equilibrium stationary state is reached, we identify the clusters and "freeze" them, i.e. we disallow any further displacements of the individuals. From that point on, the orientation of the particles is allowed to evolve according to the usual rule (Eq. (1)), but subsequent displacements (Eq. (2)) do not occur. We will refer to this stage as "restricted SVM dynamics".

In this section, we focus on single flocks, regarding them as domains that carry important information on the ordering of the system at the mesoscopic level. With this aim, we explore the relation between local topology and the ability for the restricted SVM dynamics to sustain local ordering. Clearly, with the full SVM dynamics, the onset of ordering within individual flocks is required in order to have ordered system-wide macroscopic states. However, the full SVM dynamics has an entanglement between particle displacements ("spin" translations) and XY-type interactions ("spin" rotations). By resorting to "frozen clusters", we disentangle these two major components. Notice that, although ordering in individual flocks is a necessary condition to have macroscopic system-wide ordering in the full SVM dynamics, the sufficient conditions that guarantee macroscopic order are not understood yet. We know that flocks merge, collide, and dismember, and it is by virtue of these transport mechanisms that the ordering information within one flock is carried across the system, thus resulting in effective long-range interactions [21, 30]. As shown by Toner et al. [30, 52], the spontaneous symmetry breaking of the velocity field leads to "Goldstone mode" fluctuations. In equilibrium systems, such fluctuations are strong enough to destroy the long-range order in 2 dimensions. However, the nonequilibrium effect of the nonlinear terms (which violate Galilean invariance, as expected due to the existence of a preferential reference frame) stabilize long-range ordering in the continuum model of flocking. Notice also that we are concerned with stationary states (see Sect. 2 for simulation details), hence ensemble averages are independent of time. While individual flocks (such as the one shown in Fig. 1) change over time, flock ensemble properties (such as the cluster mass distributions shown in Fig. 2) are stationary. However, the detailed mechanisms leading to the emergence of global order from locally ordered clusters are not well understood yet and remain an open question that lies beyond the scope of this work.

Figure 9 shows the dependence of the order parameter φ on the inverse cluster mass m_c^{-1}, as obtained for frozen clusters. The clusters were first generated using the full SVM dynamics with critical noise η_c. After freezing them, the restricted SVM dynamics was applied using different noise values in the $0 < \eta_f < 1$ range, as indicated. For each η_f, the corresponding order parameter plot exhibits a plateau in the $m_c^{-1} \ll 1$ region, thus indicating that a finite order parameter $\varphi_\infty > 0$ persists in the thermodynamic limit. Indeed, the order parameter in the large-cluster limit remains positive even for very large noise amplitudes, e.g. $\varphi_\infty \simeq 0.04$ for $\eta_f = 0.9$.

Let us now present additional evidence of the orientation ordering sustained by SVM frozen clusters. The symbols in Fig. 10 show the order parameter extrapolations to the $m_c^{-1} \to 0$ limit as a function of the noise amplitude η_f. For the sake of comparison, this figure also shows exact results from the mean field (i.e. fully-connected graph) solution obtained for an infinite density of individuals, namely $\varphi_{MF} = \sin(\pi\eta_f)/\pi\eta_f$ [53], which closely follows the trend of our computer simulation results. The inset to Fig. 10 shows a fit to the scaling relation $\varphi_\infty \sim |\eta_f - \eta_{f,c}|^\beta$ (dashed line) in the neighborhood of the critical frozen noise amplitude $\eta_{f,c}$. By fitting our simulation data to this relation, we find that $\beta = 1.03(5)$ and $\eta_{f,c} = 0.935(5)$. The leading term in the expansion of the mean-field solution around $(\eta_{f,c})_{MF} = 1$ leads to $\beta = 1$, in excellent agreement with the simulation results.

Figure 11(a) shows the order parameter as a function of the noise amplitude η_f for SVM frozen clusters grouped according to cluster size, as indicated. Except for the very small

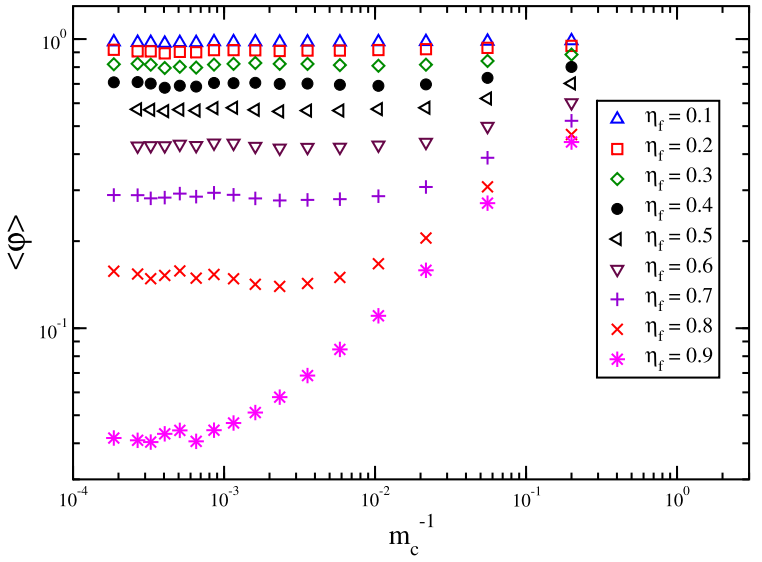

Fig. 9 Log-log plot of the order parameter as a function of the inverse cluster mass for frozen clusters with different noise levels, as indicated (Color figure online)

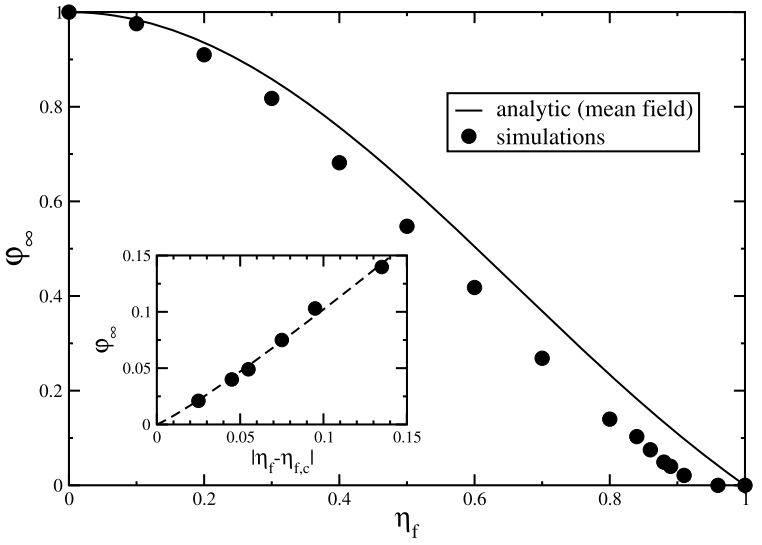

Fig. 10 Plot of the asymptotic values of the order parameter versus the noise amplitude. The *solid line* shows the mean field (i.e. fully-connected graph) results [53]. *Inset*: Simulation results (*symbols*) and fit to the data (*dashed line*), from which $\beta = 1.03(5)$ and $\eta_{f,c} = 0.935(5)$ are obtained

clusters, we observe that the ordering behavior falls into a universal curve that is essentially size-independent. Therefore, the orientation ordering signaled by $\varphi > 0$ is expected to hold for all noise amplitudes below the critical value $\eta_{f,c} = 0.935$ in the thermodynamic limit ($m_c \to \infty$). In order to complete this picture, we can perform a finite-size scaling data col-

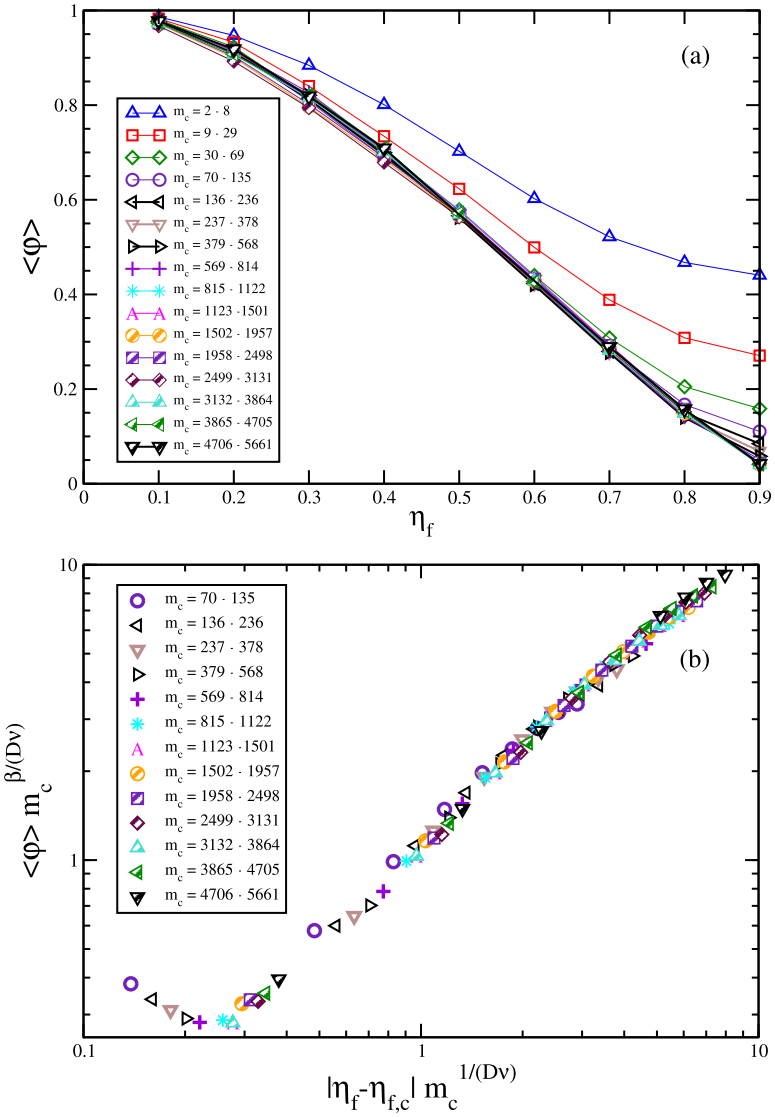

Fig. 11 (**a**) Order parameter as a function of the noise amplitude η_f for SVM frozen clusters grouped according to cluster size, as indicated. (**b**) Data collapse that shows universal behavior according to standard finite-size scaling laws of critical systems, using $\eta_{f,c} = 0.935$, $\beta = 1$, $\nu = 1$, and $D = 4$ (Color figure online)

lapse. From standard finite-size scaling theory, we know that $\langle\varphi\rangle L^{\beta/\nu} \sim |\eta_f - \eta_{f,c}|L^{1/\nu}$, where L is a characteristic linear scale of the system and ν is the exponent that characterizes the divergence of the correlation length at criticality [54]. Moreover, by combining Josephson, Rushbrooke and Fisher's critical exponent relations (see, e.g., Ref. [26]), we obtain the relation $\nu = 2\beta/(D-2)$. By replacing $\beta = 1$ (obtained from expanding the mean-field solution to leading term, which is in agreement with the fit to our data shown in the inset to Fig. 10) and $D = 4$ (the effective dimension of SVM clusters, as discussed in Sect. 3.2), we obtain $\nu = 1$. Furthermore, we can substitute $L \sim m_c^{1/D}$ in the finite-size scaling relation.

Thus, the critical behavior of the orientation of particles under the restricted SVM dynamics should manifest itself as the collapse of data from frozen clusters of different sizes when plotted as $\langle\varphi\rangle m_c^{\beta/(D\nu)} \sim |\eta_f - \eta_{f,c}| m_c^{1/(D\nu)}$ with $\eta_{f,c} = 0.935$, $\beta = 1$, $\nu = 1$, and $D = 4$. Figure 11(b) shows the data collapse that confirms the finite-size scaling behavior of the system. Based on the excellent agreement between our results and the expected behavior from finite-size scaling theory, we argue that the observed mean-field-like behavior is related to the fact that $D = 4$ is the upper-critical dimension of the XY model, which essentially has the same symmetries as the SVM defined on frozen clusters.

4 Conclusions

In this work, we presented a detailed study of the structural properties of Standard Vicsek Model (SVM) flocks from a complex network perspective. The main results are summarized in Table 1. The complex network structure of SVM flocks is characterized by a short-tailed degree distribution, very high clustering, very high assortative mixing, and nonhierarchical topology. Qualitatively, we can explain these common features as due to the intrinsic distance-driven, "ferromagnetic" nature of the Vicsek model. On the one hand, the interaction radius imposes a cutoff in the range of the particle interactions, which is reflected in the nonhierarchical topology of SVM clusters and the short-tailed degree distribution. On the other hand, the strong tendency among neighbor particles to align with each other, akin to multiple-state ferromagnets such as the XY model and resembling typical interaction mechanisms of social networks, leads to very high local clustering and assortative mixing. Based on these observations, we can characterize SVM flocks as *geographically-constrained "social" networks*.

Furthermore, the average path length dependence on cluster size shows the formation of complex structures with an effective dimension higher than that of the space where the actual displacements take place. These observations are consistent with assuming SVM clusters as 4-dimensional networked objects compactified into a $2-$dimensional space. Further support to these conclusions comes from our investigation on the onset of ordering in frozen clusters (i.e. when the particle displacements are suppressed). Indeed, we observe that frozen clusters are capable of sustaining mean-field-like orientationally ordered states (analogously to the

Table 1 Summary of results

Observable	Result
Cluster size distribution: $P \propto m_c^{-\beta_c}$	$\beta_c = 2 - 2.6$
Average path length: $APL \propto m_c^{1/D}$	$D = 4.0(2)$
Average degree distribution: $\langle k\rangle \propto m_c^{\alpha}$	$\alpha = 0.50(1)$
Degree distribution: $P(k)$ vs k	Short-tailed
Clustering coefficient distribution: $C \propto m_c^{-\gamma}$	$\gamma = 0.025(1)$
Asymptotic clustering coefficient: C_∞	$C_\infty = 0.587$
Reduced clustering coefficient distribution: $C - C_\infty \propto m_c^{-\gamma_\infty}$	$\gamma_\infty = 0.30(2)$
Hierarchical modularity: $C(k) \propto k^{-\beta_h}$	$\beta_h = 0.043(1)$
Assortative mixing: $\langle k_{\mathrm{NN}}\rangle \propto k^{-\gamma_a}$	$\gamma_a = 0.848(4)$
Assortative mixing (Pearson correlation coefficient)	$r = 0.82(6)$
Frozen clusters: $\lim_{m_c\to\infty}\varphi$	Mean Field

XY model in $4D$). This behavior is in sharp contrast with that of equilibrium systems in $2D$ space with short-range interactions and $O(2)$ symmetry defined on translationally-invariant substrates, which are indeed prevented from displaying ordered phases due to the Mermin-Wagner Theorem [27–29].

Most of the quantitative results in this work were obtained in the critical region of the SVM. A full quantitative analysis of the behavior of Vicsek flocks within the ordered phase and its dependence upon the noise amplitude would require a great computational effort that lies beyond the scope of the present paper, but remains a promising open question that would certainly deserve attention in further work.

Acknowledgements We are very grateful to F. Vázquez for fruitful discussions. This work was financially supported by CONICET, UNLP and ANPCyT (Argentina).

Appendix

Here we derive Eq. (10) for the mean clustering coefficient of a vertex in the bulk of a large cluster. Large flocks generally consist of a core that contains most of the particles and links between them distributed in a highly uniform fashion. Indeed, the near-uniform distribution of nodes and links within flock cores is not only spatial but it also manifests itself in the network's structure, as for instance shown by the short-tailed degree distributions in Fig. 4. Based on these observations and for the sake of simplicity, we assume that particles in the bulk are distributed homogeneously with a constant density ρ_{in}.

Let us recall that the clustering coefficient for node i with k_i links is defined as $C_i = 2n_i/(k_i(k_i-1))$, where n_i is the number of links between the k_i neighbors of i. Since particles are distributed uniformly within the interaction radius $R_0 = 1$, it follows straightforwardly that $k_i = \pi\rho_{\text{in}} - 1$. In order to evaluate n_i, let us focus our attention on one of the neighbor nodes of i, which we call node j. The number of nodes that are neighbors of i and j simultaneously is, on average, given by

$$n_{ij} = \rho_{\text{in}} A_{ij} - 2, \tag{14}$$

where A_{ij} is the area of the intersection between the interaction circles centered at i and j. A_{ij}, which depends only on the distance r between i and j, can be expressed as

$$A_{ij}(r) = 2\int_{-\sqrt{1-\frac{r^2}{4}}}^{\sqrt{1-\frac{r^2}{4}}} \left(\sqrt{1-x^2} - \frac{r}{2}\right) dx. \tag{15}$$

Therefore, the number of links between the k_i neighbors of i is obtained by replacing Eq. (15) in Eq. (14) and integrating $\rho_{\text{in}} n_{ij}/2$ over the unit circle (notice that we divide by 2 because we are dealing with undirected links, so we must count each pair of neighbor nodes just once), i.e.

$$n_i = \pi\rho_{\text{in}} \int_0^1 r n_{ij}(r) dr. \tag{16}$$

Solving the integrals and replacing in the definition of the clustering coefficient, we finally arrive at

$$C_\infty = \frac{[(4\pi - 3\sqrt{3})\rho_{\text{in}} - 8]\pi\rho_{\text{in}}}{4(\pi\rho_{\text{in}} - 1)(\pi\rho_{\text{in}} - 2)}, \tag{17}$$

which provides an analytic solution for the mean clustering coefficient of particles in the bulk of a large cluster.

References

1. Buhl, J., Sumpter, D.J.T., Couzin, I.D., Hale, J.J., Despland, E., Miller, E.R., Simpson, S.J.: Science **312**, 1402 (2006)
2. Szabó, B., Szölösi, G.J., Gönci, B., Jurányi, Z., Selmeczi, D., Vicsek, T.: Phys. Rev. E **74**, 061908 (2006)
3. Sokolov, A., Aranson, I.S., Kessler, J.O., Goldstein, R.E.: Phys. Rev. Lett. **98**, 158102 (2007)
4. Wu, Y., Kaiser, A.D., Jiang, Y., Alber, M.S.: Proc. Natl. Acad. Sci. **106**, 1222–1227 (2009)
5. Zhang, H.P., Be'er, A., Smith, R.S., Florin, E.L., Swinney, H.L.: Europhys. Lett. **87**, 48011 (2009)
6. Inada, Y., Kawachi, K.: J. Theor. Biol. **214**, 371 (2002)
7. Couzin, I.D., Krause, J., James, R., Ruxtony, G.D., Franks, N.R.: J. Theor. Biol. **218**, 1–11 (2002)
8. Giuggioli, L., Sevilla, F.J., Kenkre, V.M.: J. Phys. A, Math. Theor. **42**, 434004 (2009)
9. Cavagna, A., Cimarelli, A., Giardina, I., Parisi, G., Santagati, R., Stefanini, F., Viale, M.: Proc. Natl. Acad. Sci. **107**, 11865 (2010)
10. Nagy, M., Akos, Z., Biro, D., Vicsek, T.: Nature **464**, 890 (2010)
11. Helbing, D., Farkas, I., Vicsek, T.: Nature **407**, 487 (2000)
12. Faria, J.J., Dyer, J.R.G., Tosh, C.R., Krause, J.: Anim. Behav. **79**, 895 (2010)
13. Rappel, W.J., Nicol, A., Sarkissian, A., Levine, H., Loomis, W.F.: Phys. Rev. Lett. **83**, 1247 (1999)
14. Wu, X.L., Libchaber, A.: Phys. Rev. Lett. **84**, 3017 (2000)
15. Theraulaz, G., Bonabeau, E., Nicholis, S.C., Sole, R.V., Fourcassié, V., Blanco, S., Fournier, R., Joly, J.L., Fernández, P., Grimal, A., Dalle, P., Deneubourg, J.L.: Proc. Natl. Acad. Sci. **99**, 9645 (2002)
16. Feder, T.: Phys. Today **60**, 28 (2007)
17. Grančič, P., Štěpánek, F.: Phys. Rev. E **84**, 021925 (2011)
18. Vicsek, T., Zafeiris, A.: Phys. Rep. **517**, 71 (2012)
19. Vicsek, T., Czirók, A., Ben-Jacob, E., Shochet, O.: Phys. Rev. Lett. **75**, 1226 (1995)
20. Grégoire, G., Chaté, H.: Phys. Rev. Lett. **92**, 025702 (2004)
21. Aldana, M., Dossetti, V., Huepe, C., Kenkre, V.M., Larralde, H.: Phys. Rev. Lett. **98**, 095702 (2007)
22. Baglietto, G., Albano, E.V.: Phys. Rev. E **80**, 050103(R) (2009)
23. Baglietto, G., Albano, E.V., Candia, J.: Interface Focus **2**, 708 (2012)
24. Aldana, M., Huepe, C.: J. Stat. Phys. **112**, 135 (2003)
25. Binney, J.J., Dowrick, N.J., Fisher, A.J., Newman, M.E.J.: The Theory of Critical Phenomena: An Introduction to the Renormalization Group. Oxford University Press, London (1992)
26. Chaikin, P.M., Lubensky, T.C.: Principles of Condensed Matter Physics. Cambridge University Press, Cambridge (1995)
27. Mermin, N.D., Wagner, H.: Phys. Rev. Lett. **17**, 1133 (1966)
28. Mermin, N.D.: J. Math. Phys. **8**, 1061 (1967)
29. Cassi, D.: Phys. Rev. Lett. **68**, 3631 (1992)
30. Toner, J., Tu, Y.: Phys. Rev. Lett. **75**, 4326 (1995)
31. Baglietto, G., Albano, E.V.: Comput. Phys. Commun. **180**, 527 (2009)
32. Nagy, M., Daruka, I., Vicsek, T.: Physica A **373**, 445 (2007)
33. Aldana, M., Larralde, H., Vázquez, B.: Int. J. Mod. Phys. B **23**, 3661 (2009)
34. Baglietto, G., Albano, E.V.: Phys. Rev. E **78**, 021125 (2008)
35. Hoshen, J., Kopelman, R.: Phys. Rev. B **14**, 3438 (1976)
36. Newman, M.E.J., Barabási, A.L., Watts, D.J.: The Structure and Dynamics of Networks. Princeton University Press, Princeton (2006)
37. Caldarelli, G.: Scale-Free Networks: Complex Webs in Nature and Technology. Oxford University Press, London (2007)
38. Newman, M.E.J.: Networks: An Introduction. Oxford University Press, London (2010)
39. Shannon, P., Markiel, A., Ozier, O., Baliga, N.S., Wang, J.T., Ramage, D., Amin, N., Schwikowski, B., Ideker, T.: Genome Res. **13**, 2498 (2003)
40. Huepe, C., Aldana, M.: Phys. Rev. Lett. **92**, 168701 (2004)
41. Albert, R., Barabási, A.L.: Rev. Mod. Phys. **74**, 47 (2002)
42. Dorogovtsev, S.N., Goltsev, A.V., Mendes, J.F.F.: Rev. Mod. Phys. **80**, 1275 (2008)
43. Watts, D.J., Strogatz, S.H.: Nature **393**, 440 (1998)
44. Dorogovtsev, S.N., Mendes, J.F.F.: Adv. Phys. **51**, 1079 (2002)
45. Ravasz, E., Somera, A.L., Mongru, D.A., Oltvai, Z.N., Barabási, A.L.: Science **297**, 1551 (2002)
46. Ravasz, E., Barabási, A.L.: Phys. Rev. E **67**, 026112 (2003)

47. Newman, M.E.J.: Phys. Rev. Lett. **89**, 208701 (2002)
48. Newman, M.E.J.: Phys. Rev. E **67**, 026126 (2003)
49. Callaway, D.S., Hopcroft, J.E., Kleinberg, J.M., Newman, M.E.J., Strogatz, S.H.: Phys. Rev. E **64**, 041902 (2001)
50. Bordogna, C.M., Albano, E.V.: Phys. Rev. Lett. **87**, 118701 (2001)
51. Candia, J.: J. Stat. Mech. P09001 (2007)
52. Tu, Y., Toner, J., Ulm, M.: Phys. Rev. Lett. **80**, 4819 (1998)
53. Dossetti, V., Sevilla, F.J., Kenkre, V.M.: Phys. Rev. E **79**, 051115 (2009)
54. Privman, V. (ed.): Finite Size Scaling and Numerical Simulations of Statistical Systems. World Scientific, Singapore (1990)